crystals

MDPI

Article

Effects of Alloying Atoms on Antiphase Boundary Energy and Yield Stress Anomaly of $L1_2$ Intermetallics: First-Principles Study †

Xiaojun Gao [1], Jianwei Wang [2], Xiaozhi Wu [1,3,*], Rui Wang [1] and Zhihong Jia [3]

1 Institute for Structure and Function, Chongqing University, Chongqing 401331, China; 15852835163@163.com (X.G.); rcwang@cqu.edu.cn (R.W.)
2 Microsystem Technology Laboratory, Microsystem and Terahertz Research Center, CAEP, Chengdu 610200, China; wangjianwei@mtrc.ac.cn
3 College of Materials Science and Engineering, Chongqing University, Chongqing 400044, China; zhihongjia@cqu.edu.cn
* Correspondence: xiaozhiwu@cqu.edu.cn
† Project Supported by the Natural Science Foundation of China (11104361, 11647307) and Project No.CDJQJ308822 Supported by the Fundamental Research Funds for the Central Universities.

Received: 4 January 2018; Accepted: 2 February 2018; Published: 12 February 2018

Abstract: The antiphase boundary energies of {111} and {010} planes in $L1_2$ intermetallics (Ni_3Ge, Ni_3Si, Al_3Sc, Ni_3Al, Ni_3Ga and Al_3Ti) under different pressure are presented using first-principle methods. The yield stress anomaly is predicted by the energy criterion p-factor based on the anisotropy of antiphase boundary energies and elasticity. These $L1_2$ intermetallics exhibit anomalous yield stress behavior except Al_3Sc. It is found that pressure cannot introduce the transition between anomalous and normal behavior. In order to investigate the transition, Al_3Sc, Ni_3Si and Ni_3Ge with substituting atoms are investigated in detail due to p-factors of them are close to the critical value $p_c = \sqrt{3}$. Al_3Sc can change to anomalous when Sc atoms in {010} planes are substituted by Ti with plane concentration 25%. When Li substitutes Al in {111} planes, anomalous Al_3Sc will change to normal. Ni_3Si and Ni_3Ge can exhibit normal yield stress behavior when Ge and Si in {111} planes are substituted by alloying atoms with plane concentrations 12.5% and 25%. When Ga and Al substitute in {010} planes, normal Ni_3Si and Ni_3Ge will revert to anomalous behavior. Therefore, transparent transition between normal and anomalous yield stress behavior in $L1_2$ intermetallics can be introduced by alloying atoms.

Keywords: antiphase boundary energy; yield stress anomaly; $L1_2$ intermetallics; first-principle methods

1. Introduction

In materials science, the yield stress anomaly (YSA) means the yield stress of the unusual materials has a positive dependence with the increasing temperature, in contrast to the usual materials which the yield stress decreases with temperature [1–4]. $L1_2$ structure intermetallics are one kind of those materials. This property has attracted much attention for high temperature applications. For example, due to this property, $L1_2$ γ' Ni-base superalloys are widely used for blades and vanes in gas turbine engines for aircrafts and power generations [5–7].

Most models explain that the YSA in $L1_2$ intermetallics is caused by the exhaustion of the mobile dislocations on {010} planes by the Kear-Wilsdorf (K-W) locking mechanism [8–14]. The K-W locks are mainly caused by the cross-slip of the screw superdislocations [11,15,16]. With the temperature increasing, the mobile superdislocations are thermally activated to cross-slip from the {111} hexagonal

planes onto the {010} cubic planes. This process is more frequent at higher temperature. Then, it leads to the formation of K-W locks that decrease the velocity and density of the mobile dislocations. Finally the K-W locks exhaust the mobile dislocations and make the yield strength increase. Therefore, whether the materials satisfy the requirements to occur the cross-slip can be the criterion of whether they have the property of YSA. The differences of the antiphase boundary (APB) energies between {111} and {010} planes provides the driving force to form the cross-slip [17,18]. The dissociation of $\langle 110 \rangle$ superdislocation is shown as follow:

$$\langle 110 \rangle \rightarrow \frac{1}{2}\langle 110 \rangle + \mathrm{APB} + \frac{1}{2}\langle 110 \rangle \tag{1}$$

where $\langle 110 \rangle$ is the Burgers vector of superdislocations in {111} and {010} planes which will be dissociated into two $\langle 110 \rangle/2$ partials with an APB between them [19–23]. There may be other dissociation types like CSF (complex stacking fault) and SISF (superlattice intrinsic stacking fault). However, according to Schoeck et al. [24], the cross-slip can be achieved only by the recombination of two Shockley partials. Therefore here we only consider the APB energy. When the p-factor is larger than the critical value, the slip on the {111} planes will cross-slip onto the {010} planes and be divided into two $1/2[10\bar{1}]$ superpartials as shown in Figure 1. Then with the temperature increasing, the intermetallics will display anomalous behavior of yield stress. This transition from superdislocations to fully dissociated partials is examined to be related to the APB anisotropy. Therefore, the APB anisotropy ratio $\lambda = \gamma_{\{111\}}/\gamma_{\{010\}}$ is used to predict the existence of the cross-slip of $L1_2$ materials. However, Yoo considers the effect of elastic anisotropy of anisotropy materials is also important [25]. Therefore the improved energy based criterion is shown below:

$$\mathrm{p} = \frac{3\mathrm{A}}{\mathrm{A}+2}\frac{\gamma_{\mathrm{APB}}^{\{111\}}}{\gamma_{\mathrm{APB}}^{\{010\}}} > \sqrt{3} \tag{2}$$

where c_{11}, c_{12} and c_{44} are elastic constants of $L1_2$ materials, $A = 2c_{44}/(c_{11} - c_{12})$ is the elastic anisotropy, $\gamma_{\mathrm{APB}}^{\{111\}}$ is the APB energy on {111} planes and $\gamma_{\mathrm{APB}}^{\{010\}}$ is the APB energy on {010} planes. This means when the p exceeds $\sqrt{3}$, the material will have enough energy to occur cross-slip with the increasing of temperature. The material displays the behavior of YSA.

$L1_2$ structure Ni_3Al is the first material reported to have this property [11,26–29]. $L1_2$ structure Ni_3Ge [30–32], Ni_3Si [33–35] Ni_3Ga [36–38] and Al_3Ti [39] are also found to have this property. Geng et al. [40] provided a quantitative method to confirm the increase of yield strength of Ni-base superalloys at elevated temperature which is in agreement with the results of experiments. Liu et al. [41] studied the origin of the loss of the YSA of Ni_3Ge with Fe substitution. Besides $L1_2$ structure materials, many other materials are found to have this behavior. Hagihara et al. [42,43] studied $Ni_3(Ti,Nb)$ which is identified as long-period-stacking ordered (LPSO) compound in the Ni-Ti-Nb ternary system. They found the behavior of YSA is caused by basal slip in Ni-based LPSO phase and the mobility of dislocations on the non-basal plane have negligible effects. The work of Nishino et al. [44] shows that the occurrence of the YSA of $D0_3$ Fe_3Al is related to the $D0_3$-B2 phase transition. Also they studied the effects of substitutions on the phase stability and high-temperature strength. George et al. [45] explained the YSA of B2 FeAl with the vacancy-hardening model and dislocation creep at high temperatures. They also found up-quenching and down-quenching may corroborate this vacancy-hardening model through experiments. Mitchell et al. [46] studied that the YSA of $C11_b$ $MoSi_2$ is related to various slip systems and calculated the stacking fault energies with modified embedded atom method (MEAM). The work of Takayoshi et al. [47] shows the behavior of C40 $NbSi_2$ is controlled by the phase stability and the YSA is caused by the formation of a dragging atmosphere around dislocations.

In the previous work of Liu et al. [48], p-factors increasing with temperature are investigated by using first principles calculations and quasiharmonic approach. This can give a more accurate

description of the anomalous yield stress than predictions at 0 K. Pressure also has important effects on elastic constants and stacking fault energy. Therefore, it is interesting to study the pressure dependent p-factor for typical $L1_2$ intermetallics, such as Ni_3Al [27–29], Ni_3Ge [30–32], Ni_3Si [33–35], Ni_3Ga [36] and Al_3Ti [39] which have the YSA properties. To make comparisons, we also choose Al_3Sc which has the normal behavior.

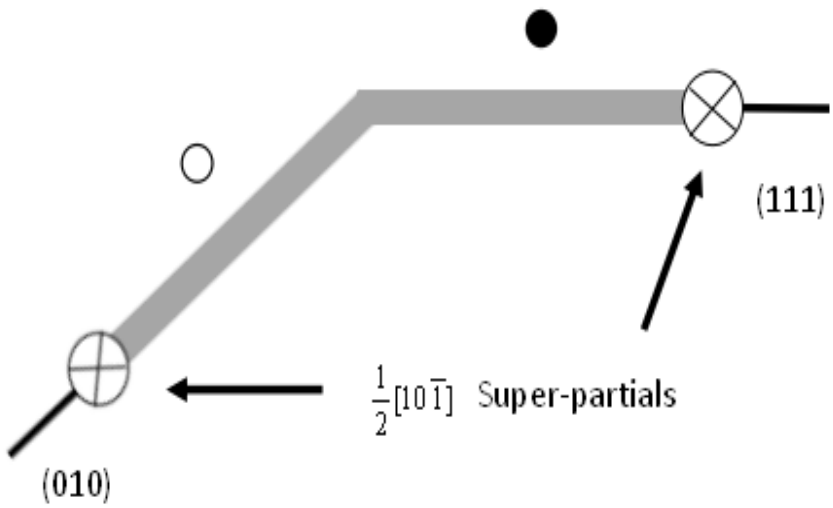

Figure 1. Structure of cross-slip from {111} onto the {010} plane. The white and black circles are substitutions on the {010} and {111} planes.

Beside pressure, alloying elements in materials also have effects on the APB energy and yield stress [44,49]. In this paper, Ni_3Ge, Ni_3Si and Al_3Sc are investigated since the p-factors of these materials are close to the critical value $p_c = \sqrt{3}$. Based on the work of Golovin et al. [50] and Balk et al. [51], the Ni_3Ge losses the property of YSA with Fe substitution. Therefore, Ni_3Ge is alloyed with Fe. Since p-factors of Ni_3Ge, Ni_3Si and Al_3Sc are close to $\sqrt{3}$, while the p-factors of Ni_3Al, Ni_3Ga and Al_3Ti are much larger than $\sqrt{3}$, Ni_3Ge is alloyed with Al and Ga, Ni_3Si is alloyed with Al, Ga and Ti, Al_3Sc is alloyed with Ti. On the other hand, since Al_3Sc is the only material that displays the normal behavior, Ni_3Ge and Ni_3Si are alloyed with Sc to investigate whether their property can be changed. Since Sc and Y, Ti and Zr are in same groups, Al_3Sc is alloyed with Y and Zr. The addition of Li in Al-Sc alloys can result in greater peak hardness from the $L1_2$ Al-Li-Sc [52]. After determining the alloying atoms, in order to confirm the alloying sites, formation energies are calculated in detail. Then, APB energies with and without alloying are calculated to obtain the p-factors.

This paper is organized as follows. The next section contains the technical details of the calculations we performed. In Section 3, we discuss our results for p-factors under different pressure. Our main results for p-factors effected by different substitutional atoms and concentrations are described in Section 4. Finally, in Section 5 we summarize the main conclusions and results.

2. Computational Methodology and Models

Calculations are performed by using the Vienna Ab-initio Simulation Package (VASP), which is based on the density functional theory (DFT). Generalized gradient approximation (GGA) with The Perdew–Burke–Ernzerhof (PBE) functional is employed as the exchange-correlation functional. All the materials calculated are $L1_2$ structures.

In cubic crystals, there are three independent elastic constants c_{11}, c_{12} and c_{44}. A $1 \times 1 \times 1$ supercell is constructed to calculate the lattice constants and the elastic constants. The cut-off energy of plane wave is set to 450 eV due to convergence test, and the Brillouin zones are performed by using Monkhorst and Pack special k points generated with a $15 \times 15 \times 15$ mesh parameters grid.

A supercell model of 12 layers perpendicular to the APB and four atoms per layer with vacuum layers is constructed to calculate APB energies in both {111} and {010} planes under the pressures of 0, 20 and 40 GPa [53]. We add vacuum layers since the vacuum layers can reduce the effects from the neighbor supercell [54]. The k points are set as 15 × 15 × 1. The structures of the {111} and {010} planes are shown in Figure 2.

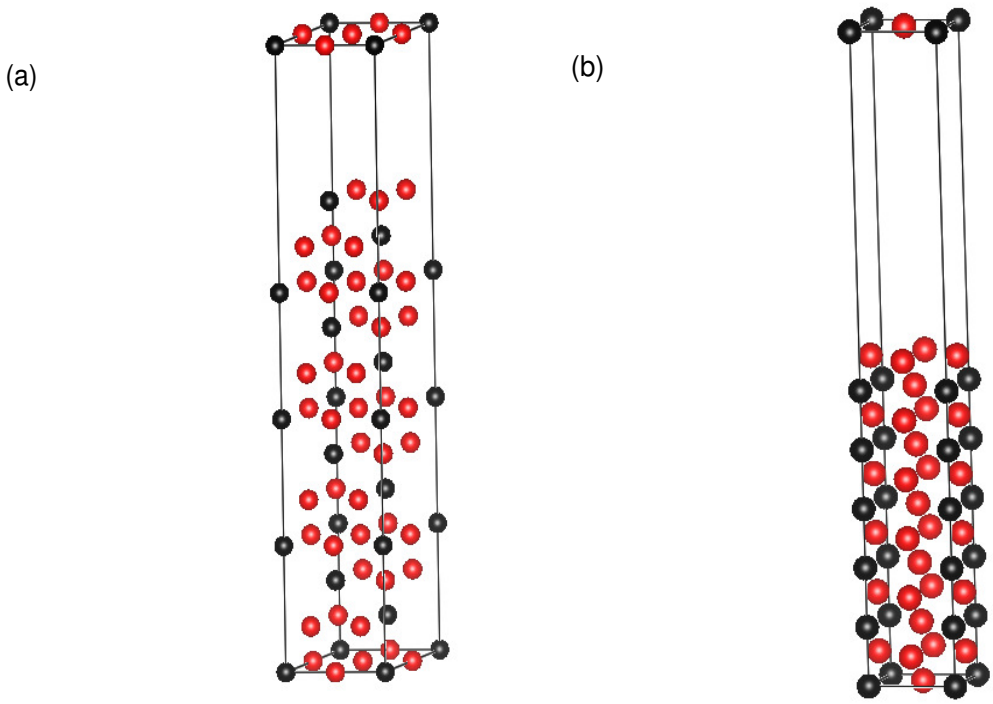

Figure 2. Supercells for antiphase boundary (APB) energy calculations in (**a**) {111} planes and (**b**) {010} planes with a concentration of 25%. Red spheres represent A atoms and black spheres represent B atoms in A_3B $L1_2$ materials.

The {111} and {010} planes with and without APB are shown in Figure 3. They are created by applying $1/2\langle 110\rangle$ shift vectors on the {111} and {010} planes or not. The APB energy γ is given by:

$$\gamma = (E_{APB} - E_0)/A_{APB} \tag{3}$$

where γ is the APB energy, E_{APB} and E_0 are the total energies of the supercell with and without APB, respectively. A_{APB} is the cross-section area of the APB. They can be calculated accurately by using first-principle methods.

When calculating the APB energies with substituting atoms, different supercells are used for different concentrations in the slip planes: 2 × 2 × 12 for a plane concentration 6.25%, 2 × 1 × 12 for a plane concentration of 12.5% and 1 × 1 × 12 for a plane concentration of 25%. All the supercells have vacuum layers. As for the Brillouin zone k-point grids, 7 × 7 × 1, 7 × 15 × 1 and 15 × 15 × 1 k-point meshes are used for different bulks.

Before calculating the APB energies, formation energies to confirm the preference of the substitutions are calculated first. Since there are different concentrations, only the supercell with the plane concentration 25% is chosen. The formation energies is given by:

$$E_f = E_{A_3B-X} - (E_A + E_B + E_X) \tag{4}$$

where E_f is the formation energy, A and B are the two kinds atoms of A_3B materials, X is the substituted atom, E_{A_3B-X} is the total energy of A_3B material with substitution, E_A, E_B and E_X are the energies of single atom of atoms A, B and substitutional atom X. By comparing the results, the most preference substitutional site can be confirmed, thus to optimize the calculations of the APB energies.

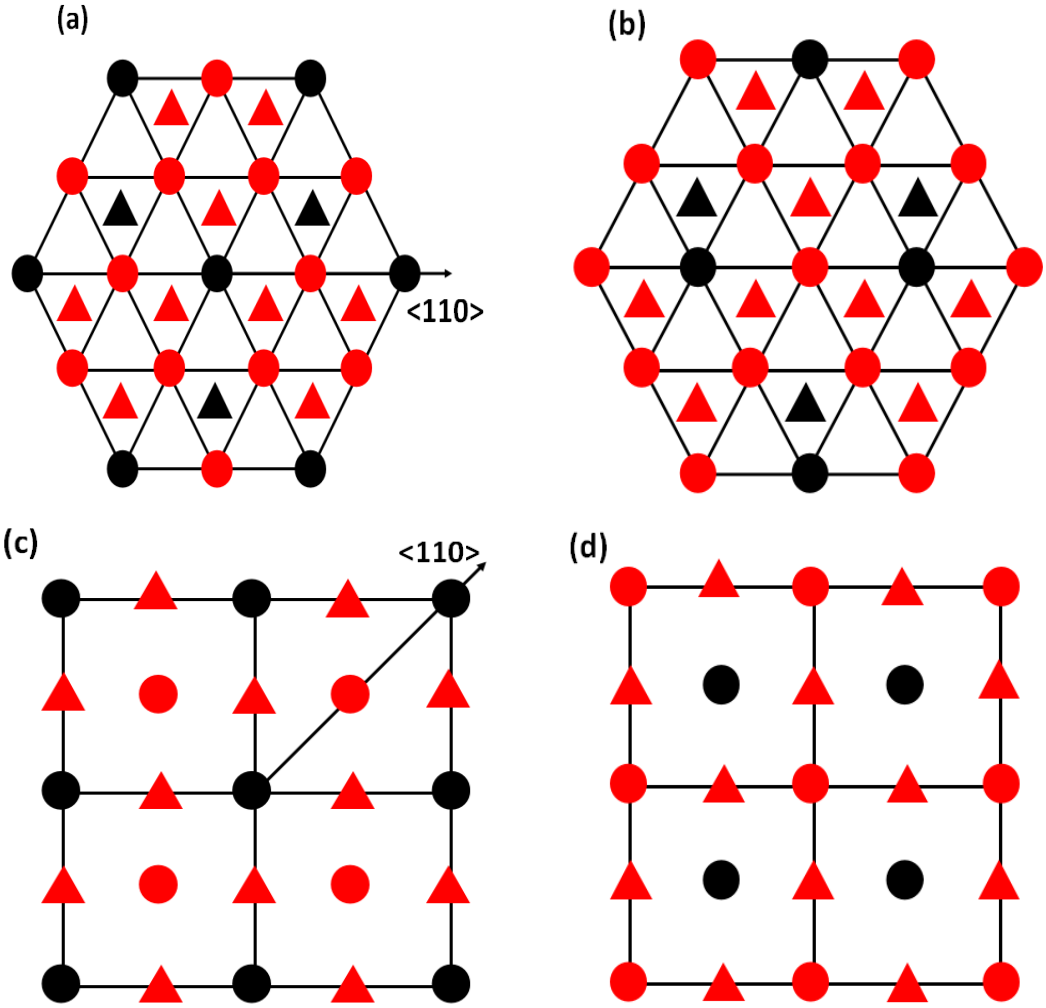

Figure 3. The atomic projection of $L1_2$ A_3B (**a**) without and (**b**) with APB on the {111} planes; (**c**) without and (**d**) with APB on the {010} planes. Red spheres represent A atoms and black spheres represent B atoms in A_3B $L1_2$ materials.

3. Effects of Pressure on Stacking Fault Energy and p-Factor

Lattice constants and elastic constants under different pressures are presented in Table 1. In general, results are in good agreement with experiments and previous theoretical calculations [55,56]. The elastic constants and anisotropy A increase with pressure. Results of A of Ni_3Al and Ni_3Ga are the larger ones, which indicate that these two materials much easily form cross-slip to have the property of YSA according to Equation (2). Specifically, it is found that the structures of Al_3Ti and Al_3Sc are not stable when P = 40 GPa. Therefore, the lattice constants and elastic constants of Al_3Ti and Al_3Sc at 40 GPa are not presented.

The APB energies in both {111} and {010} planes of Ni_3Al, Ni_3Ge, Ni_3Si, Ni_3Ga, Al_3Ti and Al_3Sc under 0, 20 and 40 GPa are shown in Table 2. Obviously, the APB energies in {010} planes are much smaller than those in {111} planes. Larger APB energy in {111} planes results in smaller dissociation

distance between partial dislocations. The possibility of construction is high for dissociated dislocation in {111} planes. Therefore, the cross-slip from {111} to {010} may be generated.

Table 1. Lattice constants a (in units of Å), elastic constants c_{11}, c_{12} and c_{44} (in units of GPa) and the elastic anisotropy ratio A of Ni_3X (X = Al, Ge, Si and Ga), Al_3X' (X′ = Ti and Sc) under different pressures P (in units of GPa).

Materials	P	a	c_{11}	c_{12}	c_{44}	*A*
Ni_3Al	0	3.569	228.42	151.76	116.89	3.05
	1.4 [55]	-	223.50	149.00	122.90	3.30
	20	3.463	330.25	231.54	161.43	3.27
	40	3.389	415.88	302.55	197.93	3.49
Ni_3Ge	0	3.585	253.81	149.28	98.83	1.89
	0 [41]	3.500	263.00	143.00	103.00	1.72
	20	3.484	367.87	231.14	141.99	2.08
	40	3.413	474.76	310.69	183.49	2.24
Ni_3Si	0	3.511	298.15	166.93	129.24	1.97
	20	3.420	410.44	247.02	174.86	2.14
	40	3.354	514.69	322.28	216.06	2.25
Ni_3Ga	0	3.588	226.66	154.68	105.40	2.93
	0 [57]	3.521	288.86	192.53	127.74	2.65
	0 [57]	3.570	264.14	169.99	116.39	2.47
	0 [58]	3.580	191.00	123.00	108.00	3.17
	20	3.482	329.99	240.69	147.18	3.30
	40	3.408	424.04	320.88	184.82	3.58
Al_3Ti	0	3.980	190.74	64.27	75.41	1.19
	0 [59]	3.985	184.40	64.21	74.61	1.24
	0 [59]	3.984	184.32	62.41	72.89	1.20
	0 [59]	3.900	207.54	69.05	87.29	1.26
	20	3.797	299.66	122.13	127.42	1.44
	20 [59]	3.799	292.10	120.50	126.80	1.48
Al_3Sc	0	4.106	182.21	39.39	71.37	1.00
	0 [60]	-	180.67	40.62	72.00	1.03
	0 [56]	4.101	187.84	35.14	73.32	0.96
	20	3.887	293.69	94.29	124.15	1.25
	20 [56]	-	312.83	88.19	128.13	1.14

Based on the calculated APB energies and elastic constants, the anomalous yield stress phenomenon is predicted by the energy-based criterion Equation (2). The p-factors of Ni_3Al, Ni_3Ge, Ni_3Si, Ni_3Ga, Al_3Ti and Al_3Sc under the different pressures are shown in Figure 4. Noticeably, the calculated p-factor of Ni_3Si at 0 GPa is lower than $\sqrt{3}$, which is in agreement with Yoo [61]. However, based on the observed behavior of YSA for Ni_3Si, Yoo still considers Ni_3Si to have a positive temperature dependence of yield stress, and by calculating with other supercells, the p-factor of Ni_3Si satisfies the criterion. Therefore, here, Ni_3Si is regarded to have the property of YSA at 0 GPa, as well. According to Equation (2), although the A of Al_3Ti, Ni_3Al and Ni_3Ga increases with pressure (see Table 1), due to the APB energy in {010} planes having a faster growth than the one in {111} planes, p-factors of Al_3Ti, Ni_3Al and Ni_3Ga keep decreasing with pressure, and they are still much larger than $\sqrt{3}$ among all pressures. The values of p-factors of Al_3Sc, Ni_3Ge and Ni_3Si increase with pressure, and the A of them has the same trend of increase. This indicates that APB energy in {010} planes does not have many effects on the changes of the p-factor with pressure. The changes of the p-factors of Ni_3Ge and Ni_3Si are not obvious, and the values are still slightly larger than $\sqrt{3}$. These results mean they all exhibit the YSA under all pressures investigated here. On the other hand, only the p-factor of Al_3Sc is smaller than $\sqrt{3}$ under all pressures, which means this material does not have YSA; although

it increases slightly with pressure. All these results are in good agreement with the properties achieved from experiments. This means pressure has negligible influence on the property of yield stress.

Table 2. APB energies (in units of J/m^2) on {111} and {010} planes of Ni_3X (X = Al, Ge, Si and Ga), Al_3X' (X′ = Ti and Sc) under different pressures P (in units of GPa). λ (ratio of APB_{111}/APB_{010}) and p-factors are also presented.

Materials	P	0	20	40
Ni_3Al	{111}	0.344	0.406	0.459
	{010}	0.117	0.173	0.205
	λ	2.940	2.346	2.239
	p	5.352	4.626	4.282
Ni_3Ge	{111}	0.509	0.587	0.651
	{010}	0.381	0.415	0.442
	λ	1.336	1.414	1.473
	p	1.950	2.163	2.331
Ni_3Si	{111}	0.455	0.515	0.565
	{010}	0.395	0.453	0.506
	λ	1.152	1.137	1.117
	p	1.718	1.766	1.777
Ni_3Ga	{111}	0.272	0.308	0.337
	{010}	0.016	0.024	0.029
	λ	17.000	12.833	11.621
	p	31.396	24.485	22.320
Al_3Ti	{111}	0.258	0.643	-
	{010}	0.094	0.173	-
	λ	2.745	3.717	-
	p	5.615	4.748	-
Al_3Sc	{111}	0.741	1.025	-
	{010}	0.575	0.851	-
	λ	1.289	1.204	-
	p	1.280	1.394	-

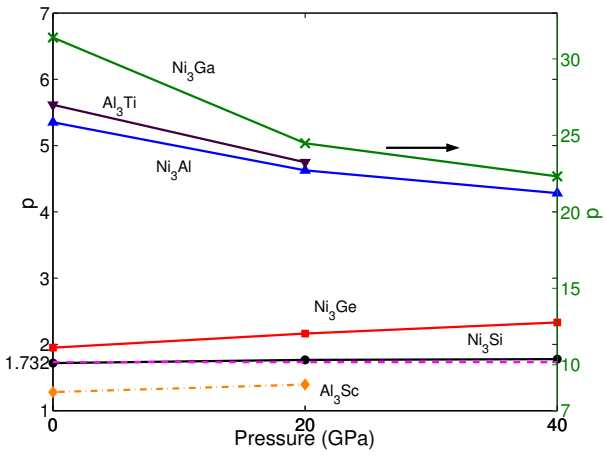

Figure 4. p of Ni_3X (X = Al, Ge, Si and Ga) and Al_3X' (X′ = Ti and Sc) under different pressures p = 0, 20 and 40 GPa. The blue solid line with up-triangles shows the results of Ni_3Al. The red solid line with squares shows the results of Ni_3Ge. The black solid line with circles shows the results of Ni_3Si. The green solid line with crosses shows the results of Ni_3Ga, which is shown by the right axis. The brown solid line with down-triangles shows the results of Al_3Ti. The yellow dashed-dotted line with diamonds shows the results of Al_3Sc. The magenta dash line represents the critical value of $p_c = \sqrt{3}$.

4. Effects of Substituting Atoms on Stacking Fault Energy and p-Factor

4.1. Substituted by a Single Atom

Based on the above results, the pressure will not introduce the transition between anomalous and normal behavior. In this section, the effects of substitutional atoms on p-factor will be investigated. p-factors of Ni_3Ge, Ni_3Si and Al_3Sc are studied since they are close to $\sqrt{3}$. In Figure 1, there are substitutions (black circle and white circle) on either {111} and {010} planes, which affect the $\gamma_{APB}^{\{111\}}$ and $\gamma_{APB}^{\{010\}}$. Therefore, as discussed above, Ni_3Ge is substituted with Fe, Sc, Al or Ga, Ni_3Si is substituted with Al, Ga, Ti or Sc and Al_3Sc is substituted with Ti, Y, Zr or Li.

To determine the substitutional sites, the formation energies of Ni_3Ge, Ni_3Si and Al_3Sc with alloying atoms are presented. All possible substitutional sites are taken into consideration. Results of the formation energies of different substitution sites are shown in Table 3. It is easy to see that: (1) the formation energies of Sc_{Ge}, Al_{Ge} Ga_{Ge} and Fe_{Ni} are lower to make the structure more stable; (2) the formation energies of Sc_{Si}, Ti_{Si} Ga_{Si} and Al_{Si} are lower to make the structure more stable; (3) the formation energies of Ti_{Sc}, Y_{Sc} and Zr_{Sc} and Li_{Al} are lower to make the structure more stable. Fe_{Ni} means that the Ni site is substituted by Fe, and so forth. Therefore, Sc, Al and Ga tend to occupy the site of Ge, while Fe tends to occupy the site of Ni in Ni_3Ge. Al, Ga, Ti and Sc all tend to occupy the site of Si in Ni_3Si. Ti, Y and Zr tend to occupy the site of Sc, while Li tends to occupy the site of Al in Al_3Sc.

Table 3. Formation energies (in units of eV) of Ni_3Ge substituted with Fe on Ni sublattice and Sc, Al, Ga on the Ge sublattice. Energies of substituted Ni_3Si and Al_3Sc are presented, as well.

Ni_3Ge	Fe	Sc	Al	Ga
Ni	−36.21	−32.22	−32.89	−32.25
Ge	−34.69	−33.02	−33.52	−33.01
Ni_3Si	Al	Ga	Ti	Sc
Ni	−53.90	−53.23	−53.58	−52.64
Si	−54.02	−53.43	−53.87	−52.98
Al_3Sc	Ti	Y	Li	Zr
Al	−50.86	−49.45	−50.86	−50.41
Sc	−51.15	−51.15	−49.46	−51.63

Three different plane concentrations of 6.25%, 12.5%, and 25% are used to calculate the APB energies. APB energies in {111} and {010} planes are shown in Table 4. It is interesting to find that substitutional atoms decrease APB energies in {111} planes except Zr_{Sc} in Al_3Sc. The APB energies in {010} planes are also decreased by substitutional atoms except Fe_{Ni}, Sc_{Si}, Y_{Sc} and Li_{Al}.

Based on APB energies, p-factors of Ni_3Ge, Ni_3Si and Al_3Sc at different concentrations are obtained (see Tables 4 and 5). Table 4 shows the p-factor of atoms substituted in both {111} and {010} planes, and Table 5 shows the p-factor of atoms substituted only in {111} or {010} planes, respectively.

The p-factors of YSA for Ni_3Ge with substitutional atoms are shown in Figure 5. $Fe_{Ni}^{\{111\}}$ means Ni substituted by Fe only in {111} planes; $Fe_{Ni}^{\{010\}}$ means Ni substituted by Fe only in {010} planes; and $Fe_{Ni}^{\{111\}\&\{010\}}$ means Ni substituted by Fe both in {111} and {010} planes, and so forth. It is transparent that when only substituting atoms in {111} planes, the p-factors of $Fe_{Ni}^{\{111\}}$, $Sc_{Ge}^{\{111\}}$, $Al_{Ge}^{\{111\}}$ and $Ga_{Ge}^{\{111\}}$ decrease with the concentrations. These are originated from the decrease of APB energies of Ni_3Ge with substitutional atoms in {111} planes (see Table 4). When the concentration is 12.5%, Ni_3Ge will display the normal behavior with $Sc_{Ge}^{\{111\}}$ or $Al_{Ge}^{\{111\}}$. With the concentration increasing to 25%, $Ga_{Ge}^{\{111\}}$ can change the property of YSA for Ni_3Ge, as well. When only substituting atoms in {010} planes, the p-factors of $Sc_{Ge}^{\{010\}}$, $Al_{Ge}^{\{010\}}$ and $Ga_{Ge}^{\{010\}}$ increase, and the properties of YSA for Ni_3Ge are enhanced due to the decrease of APB energies in {010} planes with substitutions; except that $Fe_{Ni}^{\{010\}}$ weakens the properties of YSA with the plane concentration increasing from 12.5%–25% due to the APB energy

increasing from 0.412 J/m^2–0.478 J/m^2. When substituting atoms in both {111} and {010} planes, p-factors lie between those that only substitute in {111} or {010} planes. Due to the lower decrease of the APB energies of $Sc_{Ge}^{\{010\}}$ compared to the APB energies in {111} planes than those of Al_{Ge} and Ga_{Ge}, the p-factor of $Sc_{Ge}^{\{111\}\&\{010\}}$ at a concentration of 25% is the only one less than the critical value to make Ni_3Ge show the normal behavior.

Table 4. The APB energies (in units of J/m^2) of {111} and {010} planes in Ni_3Ge, Ni_3Si and Al_3Sc with different substitutional concentrations (0%, 6.25%, 12.5% and 25%). p-factors of atoms substituted in or both planes are also presented. Fe_{Ni} means that the Ni site is substituted by Fe, and so forth.

Materials	Substitutions	$APB_{\{111\}}$				$APB_{\{010\}}$				$P_{\{111\}\&\{010\}}$			
		0%	6.25%	12.5%	25%	0%	6.25%	12.5%	25%	0%	6.25%	12.5%	25%
Ni_3Ge	Fe_{Ni}	0.691	0.665	0.643	0.621	0.515	0.434	0.412	0.478	1.955	2.235	2.278	1.895
	Sc_{Ge}	0.691	0.628	0.566	0.442	0.515	0.477	0.465	0.431	1.955	1.919	1.774	1.497
	Al_{Ge}	0.691	0.648	0.600	0.494	0.515	0.469	0.424	0.295	1.955	2.014	2.064	2.443
	Ga_{Ge}	0.691	0.655	0.613	0.519	0.515	0.467	0.417	0.277	1.955	2.044	2.143	2.732
Ni_3Si	Al_{Si}	0.666	0.635	0.602	0.523	0.520	0.507	0.464	0.351	1.831	1.866	1.931	2.219
	Ga_{Si}	0.666	0.641	0.614	0.548	0.520	0.500	0.450	0.317	1.831	1.907	2.031	2.575
	Ti_{Si}	0.666	0.631	0.609	0.577	0.520	0.506	0.505	0.480	1.831	1.855	1.796	1.792
	Sc_{Si}	0.666	0.629	0.596	0.530	0.520	0.518	0.521	0.545	1.831	1.806	1.704	1.449
Al_3Sc	Ti_{Sc}	0.698	0.666	0.637	0.562	0.558	0.527	0.472	0.343	1.251	1.262	1.349	1.637
	Y_{Sc}	0.698	0.738	0.775	0.697	0.558	0.600	0.630	0.696	1.251	1.229	1.228	1.001
	Li_{Al}	0.698	0.669	0.630	0.558	0.558	0.568	0.582	0.604	1.251	1.177	1.083	0.924
	Zr_{Sc}	0.698	0.704	0.708	0.718	0.558	0.557	0.529	0.454	1.251	1.239	1.337	1.581

Table 5. p-factors for Ni_3Ge, Ni_3Si and Al_3Sc with atoms only substituted in the {111} or {010} planes.

Materials	Substitutions	$P_{\{111\}}$				$P_{\{010\}}$		
		0	6.25%	12.5%	25%	6.25%	12.5%	25%
Ni_3Ge	Fe_{Ni}	1.955	1.883	1.820	1.758	2.320	2.447	2.108
	Sc_{Ge}	1.955	1.789	1.609	1.253	2.110	2.168	2.337
	Al_{Ge}	1.955	1.845	1.708	1.399	2.147	2.376	3.415
	Ga_{Ge}	1.955	1.865	1.743	1.470	2.155	2.419	3.635
Ni_3Si	Al_{Si}	1.831	1.746	1.657	1.499	1.951	2.139	2.826
	Ga_{Si}	1.831	1.763	1.670	1.569	1.975	2.207	3.133
	Ti_{Si}	1.831	1.736	1.677	1.654	1.952	1.966	2.068
	Sc_{Si}	1.831	1.729	1.641	1.518	1.907	1.907	1.822
Al_3Sc	Ti_{Sc}	1.251	1.175	1.134	1.007	1.327	1.487	2.035
	Y_{Sc}	1.251	1.304	1.379	1.250	1.166	1.113	1.002
	Li_{Al}	1.251	1.182	1.122	1.001	1.232	1.206	1.155
	Zr_{Sc}	1.251	1.244	1.261	1.288	1.257	1.325	1.536

The p-factors of YSA for Ni_3Si with substitutional atoms are shown in Figure 6. It is transparent that p-factors of substituting atoms only in {111} planes decrease with concentrations of $Al_{Si}^{\{111\}}$, $Ga_{Si}^{\{111\}}$, $Ti_{Si}^{\{111\}}$ and $Sc_{Si}^{\{111\}}$. These are originated from the decrease of APB energies of Ni_3Si with the substitutional atoms in {111} planes (see Table 4). Ni_3Si starts to display the normal behavior when the plane concentrations are 12.5%. However, when substituting atoms only in {010} planes, the properties of YSA for Ni_3Si are enhanced by $Al_{Si}^{\{010\}}$, $Ga_{Si}^{\{010\}}$ or $Ti_{Si}^{\{010\}}$ due to the decreasing of APB energies in {010} planes with substitutions. Only when Sc is substituted in {010} planes, since the APB energy increases from 0.521 J/m^2–0.545 J/m^2, while plane concentration increases from 12.5%–25%, the p-factor decreases. Due to the decrease of APB energies of Al_{Si}, Ga_{Si}, Ti_{Si} in both planes, p-factors of atoms substituted in both planes lie between those of substituting in a single plane. Only the p-factor of $Sc_{Si}^{\{111\}\&\{010\}}$ stays lower than Sc_{Si} in {010} planes to display the normal behavior when the concentration is larger than 12.5%. This is caused by the increase of APB energies in {010} planes and the decrease of APB energies in {111} planes.

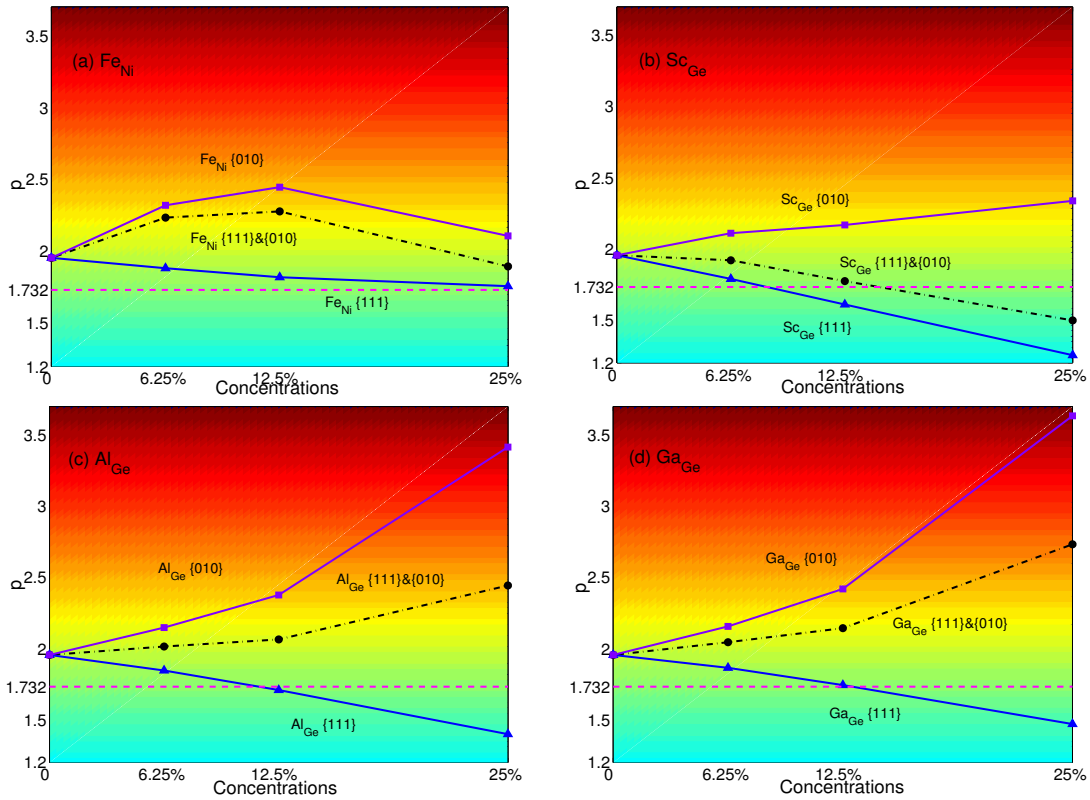

Figure 5. p-factors of Ni_3Ge substituted with (**a**) Fe; (**b**) Sc; (**c**) Al; and (**d**) Ga. Black dashed-dotted lines with circles represent the results of atoms substituted in both {111} and {010} planes; blue solid lines with triangles represent the results of atoms substituted only in {111} planes; purple solid lines with squares represent the results of atoms substituted only in {010} planes. Magenta dashed lines represent the critical value of $p_c = \sqrt{3}$.

The p-factors of YSA for Al_3Sc with substitutional atoms are shown in Figure 7. It is transparent that the p-factors of substituting atoms only in {111} planes decrease with increasing concentrations of $Ti_{Sc}^{\{111\}}$ or $Li_{Al}^{\{111\}}$. These are due to the decrease of APB energies of Al_3Sc with substituting Li or Ti in {111} planes (see Table 4). The p-factor of $Zr_{Sc}^{\{111\}}$ has few changes. Besides, the p-factor of $Y_{Sc}^{\{111\}}$ increases since the APB energy of $Y_{Sc}^{\{111\}}$ increases from 0.698 J/m^2–0.775 J/m^2 while the plane concentration increases from 0–12.5%. Then, it decreases with the APB energy decreasing to 0.697 J/m^2 when the plane concentration reaches 25%. When atoms are substituted only in {010} planes, the p-factors of $Ti_{Sc}^{\{010\}}$ and $Zr_{Sc}^{\{010\}}$ increase with concentrations, while $Li_{Al}^{\{010\}}$ and $Y_{Sc}^{\{010\}}$ have different trends. Al_3Sc displays the anomalous behavior only when substituting Ti in {010} planes with the plane concentration of 25%. Due to the APB energies of Ti_{Sc} in both planes increasing with concentrations, p-factors of $Ti_{Sc}^{\{111\}\&\{010\}}$ lie between those of substituting in single plane. p-factors of $Y_{Sc}^{\{111\}\&\{010\}}$ are similar to those of $Ti_{Sc}^{\{111\}\&\{010\}}$ at the plane concentration of 12.5%. Due to the APB energies of Li_{Al} increasing in {010} planes and decreasing in {111} planes, the p-factors of $Li_{Al}^{\{111\}\&\{010\}}$ keep decreasing with concentrations. From Figure 7c, the p-factor of $Li_{Al}^{\{111\}\&\{010\}}$ lies below the other two and is the lowest at all concentrations. On the other hand, the increase of APB energies of $Zr_{Sc}^{\{111\}}$ and the decrease of APB energies of $Zr_{Sc}^{\{010\}}$ lead to the p-factor of $Zr_{Sc}^{\{111\}\&\{010\}}$ to become the highest. However, none of these p-factors with atoms substituted in both planes can reach the critical value at all concentrations.

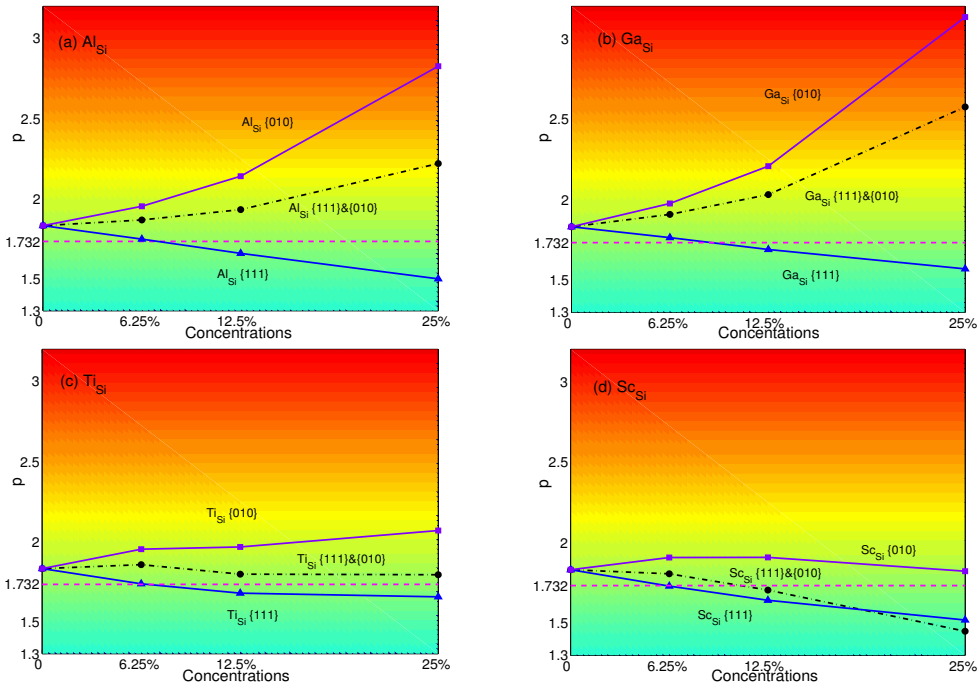

Figure 6. p-factors of Ni_3Si substituted by (**a**) Al; (**b**) Ga; (**c**) Ti; and (**d**) Sc. Black dashed-dotted lines with circles represent the results of atoms substituted in both {111} and {010} planes; blue solid lines with triangles represent the results of atoms substituted only in {111} planes; purple solid lines with squares represent the results of atoms substituted only in {010} planes. Magenta dash lines represent the critical value of $p_c = \sqrt{3}$.

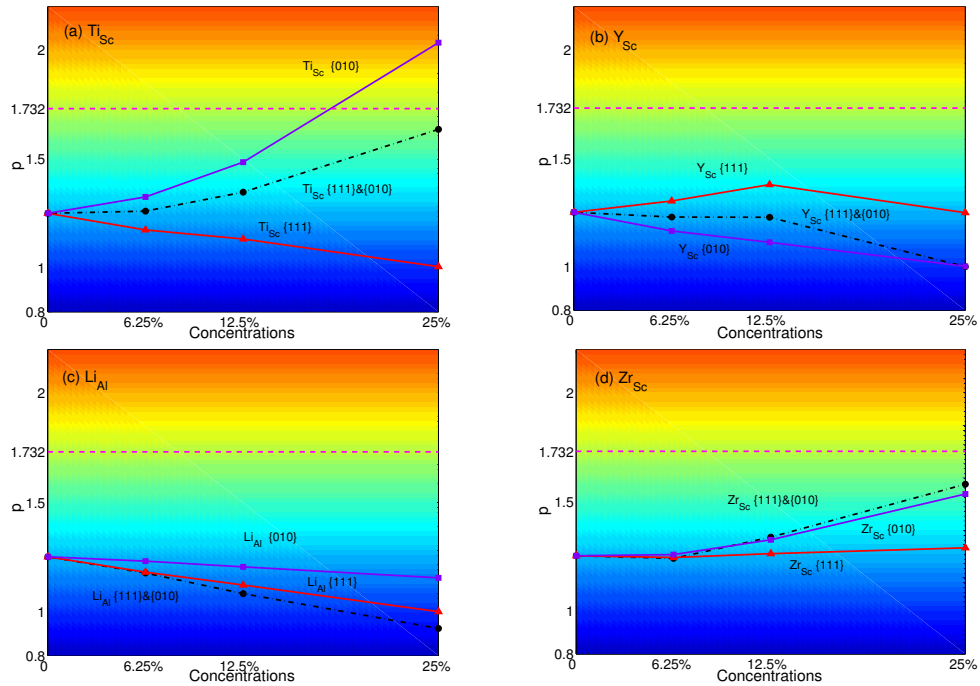

Figure 7. p-factors of Al_3Sc: substituted with (**a**) Ti; (**b**) Y; (**c**) Li; and (**d**) Zr. Black dashed-dotted lines with circles represent the results of atoms substituted in both {111} and {010} planes; red solid lines with triangles represent the results of atoms substituted only in {111} planes; purple solid lines with squares represent the results of atoms substituted only in {010} planes. Magenta dashed lines represent the critical value of $p_c = \sqrt{3}$.

Comparing the different concentrations, the effects of substitutional atoms are enhanced with increasing concentrations. When the concentration is 12.5%, it makes the effects of atom substituted in {111} planes great enough to change the behavior from anomalous to normal obvious, such as $Sc_{Ge}^{\{111\}}$, $Al_{Si}^{\{111\}}$, $Ga_{Si}^{\{111\}}$, $Ti_{Si}^{\{111\}}$ and $Sc_{Si}^{\{111\}}$. When the concentration is 25%, $Ti_{Sc}^{\{010\}}$ can be effective enough to make Al_3Sc have the property of YSA.

4.2. Substituted by Two Different Atoms

In this section, different alloying atoms are substituted in the {111} and {010} planes of Ni_3Ge, Ni_3Si and Al_3Sc with the same concentrations. The p-factors are plotted in Figures 8–10.

The p-factors of Ni_3Ge are plotted in Figure 8: (a) $Fe_{Ni}^{\{111\}}$ with $Sc_{Ge}^{\{010\}}$ (black dashed-dotted line with circles), $Al_{Ge}^{\{010\}}$ (blue solid line with triangles) and $Ga_{Ge}^{\{010\}}$ (purple solid line with squares); (b) $Sc_{Ge}^{\{111\}}$ with $Al_{Ge}^{\{010\}}$ (blue solid line with triangles), $Ga_{Ge}^{\{010\}}$ (purple solid line with squares) and $Fe_{Ni}^{\{010\}}$ (black dashed-dotted line with circles); (c) $Al_{Ge}^{\{111\}}$ with $Sc_{Ge}^{\{010\}}$ (blue solid line with triangles), $Ga_{Ge}^{\{010\}}$ (purple solid line with squares) and $Fe_{Ni}^{\{010\}}$ (black dashed-dotted line with circles); (d) $Ga_{Ge}^{\{111\}}$ with $Sc_{Ge}^{\{010\}}$(blue solid line with triangles), $Al_{Ge}^{\{010\}}$ (purple solid line with squares) and $Fe_{Ni}^{\{010\}}$ (black dashed-dotted line with circles), respectively.

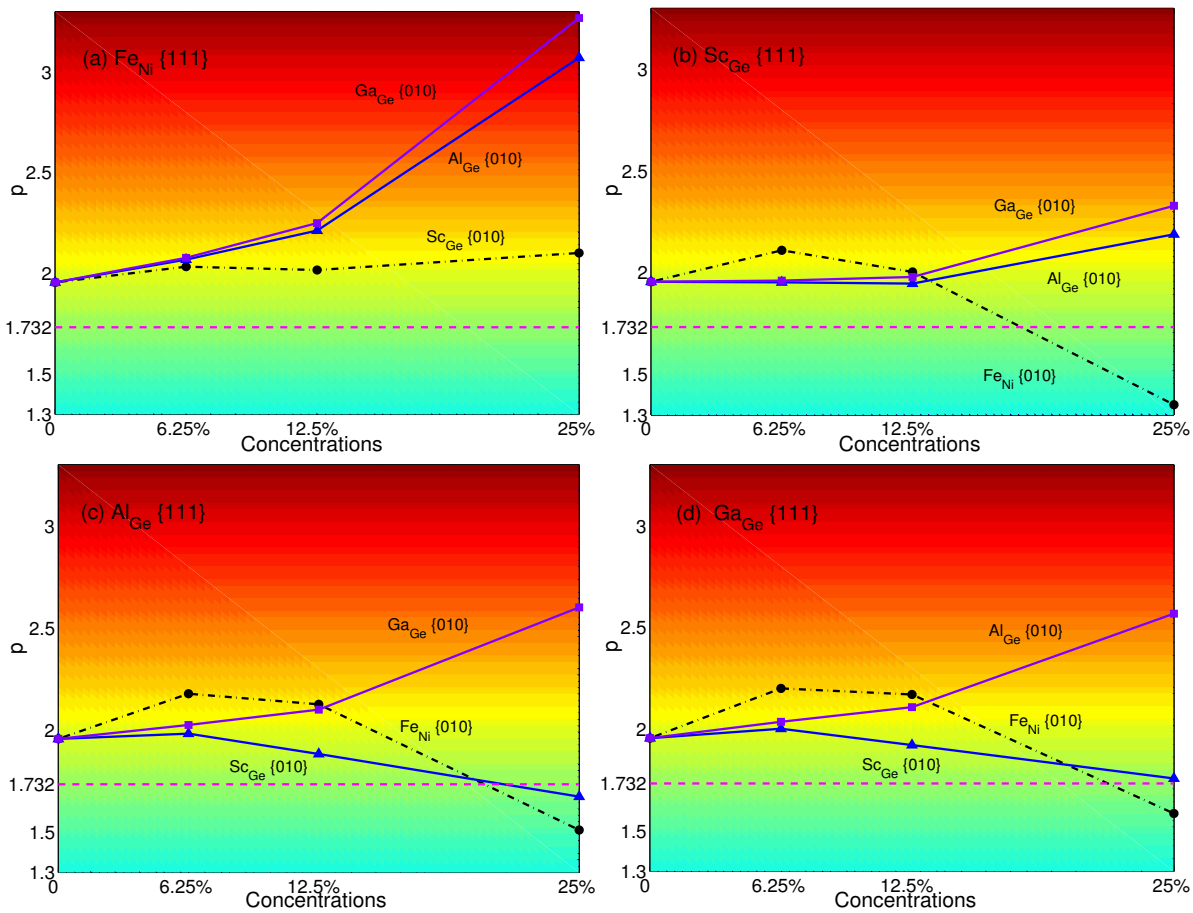

Figure 8. p-factors of Ni_3Ge: (**a**) Fe_{Ni} in {111} planes with Sc_{Ge}, Al_{Ge} and Ga_{Ge} in {010} planes; (**b**) Sc_{Ge} in {111} planes with Fe_{Ni}, Al_{Ge} and Ga_{Ge} in {010} planes; (**c**)Al_{Ge} in {111} planes with Fe_{Ni}, Sc_{Ge} and Ga_{Ge} in {010} planes; (d) Ga_{Ge} in {111} planes with Fe_{Ni}, Sc_{Ge} and Al_{Ge} in {010} planes. Magenta dash lines represent the critical value of $p_c = \sqrt{3}$.

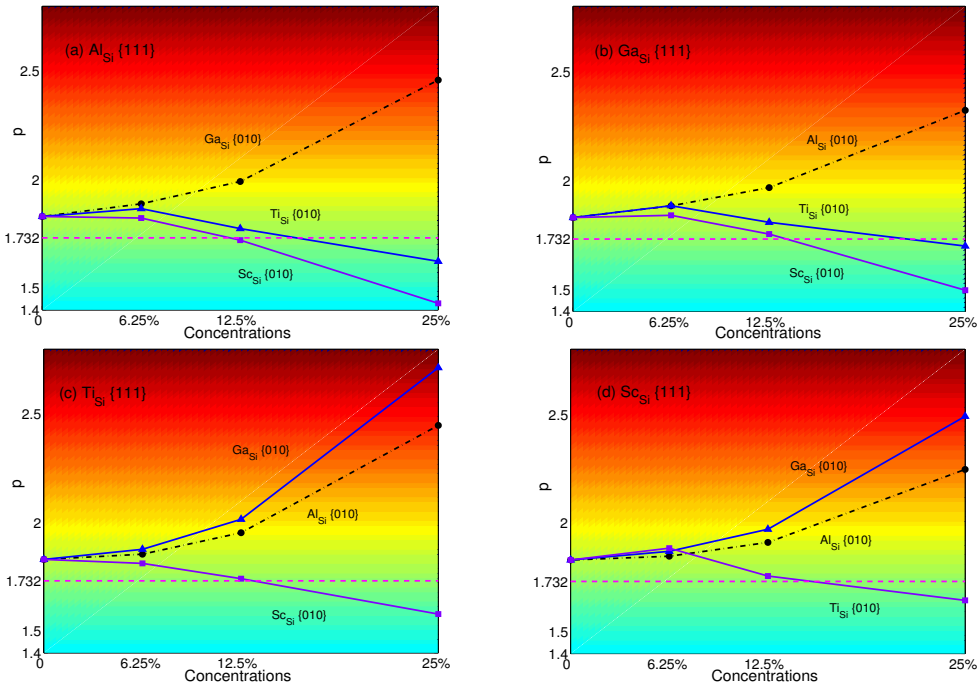

Figure 9. p-factors of Ni_3Si: (**a**) Al_{Ge} in {111} planes with Ga_{Si}, Ti_{Si} and Sc_{Si} in {010} planes; (**b**) Ga_{Si} in {111} planes with Al_{Si}, Ti_{Si} and Sc_{Si} in {010} planes; (**c**) Ti_{Si} in {111} planes with Al_{Si}, Sc_{Si} and Sc_{Si} in {010} planes; (**d**) Sc_{Si} in {111} planes with Al_{Si}, Ga_{Si} and Ti_{Si} in {010} planes. Magenta dash lines represent the critical value of $p_c = \sqrt{3}$.

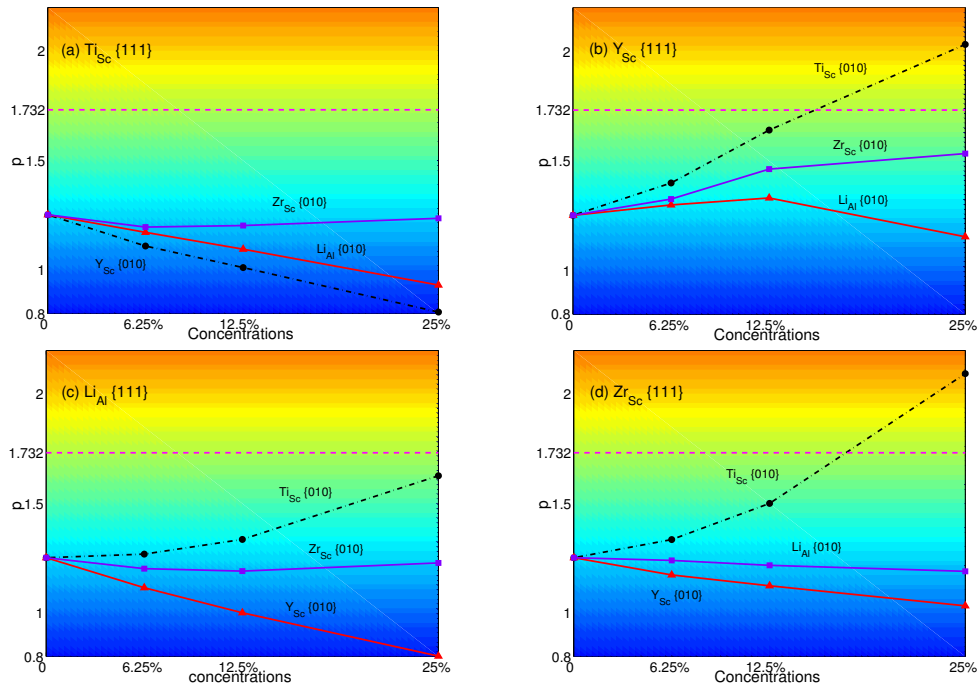

Figure 10. p-factors of Al_3Sc: (**a**) Ti_{Sc} in {111} planes with Y_{Sc}, Li_{Al} and Zr_{Sc} in {010} planes; (**b**) Y_{Sc} in {111} planes with Ti_{Sc}, Li_{Al} and Zr_{Sc} in {010} planes; (**c**) Li_{Al} in {111} planes with Ti_{Sc}, Y_{Sc} and Zr_{Sc} in {010} planes; (**d**) Zr_{Sc} in {111} planes with Ti_{Sc}, Y_{Sc} and Li_{Al} in {010} planes. Magenta dash lines represent the critical value of $p_c = \sqrt{3}$.

From Figure 8, it is easy to see that the transition of Ni_3Ge does not exist when $Fe_{Ni}^{\{111\}}$ with $Ga_{Ge}^{\{010\}}$, $Al_{Ge}^{\{010\}}$ or $Sc_{Ge}^{\{010\}}$. p-factors of $Sc_{Ge}^{\{111\}}$ with $Ga_{Ge}^{\{010\}}$ or $Al_{Ge}^{\{010\}}$, $Al_{Ge}^{\{111\}}$ with $Ga_{Ge}^{\{010\}}$ and $Ga_{Ge}^{\{111\}}$ with $Al_{Ge}^{\{010\}}$ have the same trend of increase, which means their properties of YSA will not be changed. Besides, the p-factor of $Ga_{Ge}^{\{111\}}$ with $Sc_{Ge}^{\{010\}}$ decreases with concentrations. Though the p-factor of it is very close to $\sqrt{3}$ at a plane concentration of 25%, it is still slightly higher than $\sqrt{3}$, which means that there is no transition from anomalous to normal. $Sc_{Ge}^{\{111\}}$ with $Fe_{Ni}^{\{010\}}$, $Al_{Ge}^{\{111\}}$ with $Fe_{Ni}^{\{010\}}$ or $Sc_{Ge}^{\{010\}}$ and $Ga_{Ge}^{\{111\}}$ with $Fe_{Ni}^{\{010\}}$ will result in transition with a plane concentration of 25%. It can be found that $Fe_{Ni}^{\{010\}}$ will decrease the p-factors with the concentration varying from 6.25%–25% no matter whether there are atoms substituted in {111} planes; only $Fe_{Ni}^{\{111\}}$ can lead to a small increase of p-factor with the concentration varying from 6.25%–12.5% (see Figure 5a). Additionally, it will be small enough to change the property of yield stress from anomalous to normal at the concentration of 25%. Comparing with Figures 5 and 8, it can be seen that substituting Al or Ga in {010} planes with a concentration of 25% can be effective to revert the normalized Ni_3Ge with $Sc_{Ge}^{\{111\}}$, $Al_{Ge}^{\{111\}}$ or $Ga_{Ge}^{\{111\}}$ to anomalous.

The p-factors of Ni_3Si are plotted in Figure 9: (a) $Al_{Si}^{\{111\}}$ with $Ga_{Si}^{\{010\}}$ (black dashed-dotted line with circles), $Ti_{Si}^{\{010\}}$(blue solid line with triangles) and $Sc_{Si}^{\{010\}}$ (purple solid line with squares); (b) $Ga_{Si}^{\{111\}}$ with $Al_{Si}^{\{010\}}$ (black dashed-dotted line with circles), $Ti_{Si}^{\{010\}}$ (blue solid line with triangles) and $Sc_{Si}^{\{010\}}$ (purple solid line with squares); (c) $Ti_{Si}^{\{111\}}$ with $Al_{Si}^{\{010\}}$ (black dashed-dotted line with circles), $Ga_{Si}^{\{010\}}$ (blue solid line with triangles) and $Sc_{Si}^{\{010\}}$ (purple solid line with squares); (d) $Sc_{Si}^{\{111\}}$ with $Al_{Si}^{\{010\}}$ (black dashed-dotted line with circles), $Ga_{Si}^{\{010\}}$ (blue solid line with triangles) and $Ti_{Si}^{\{010\}}$ (purple solid line with squares), respectively.

From Figure 9, it is easy to see that $Al_{Si}^{\{111\}}$ with $Ga_{Si}^{\{010\}}$, $Ga_{Si}^{\{111\}}$ with $Al_{Si}^{\{010\}}$, $Ti_{Si}^{\{111\}}$ with $Ga_{Si}^{\{010\}}$ or $Al_{Si}^{\{010\}}$ and $Sc_{Si}^{\{111\}}$ with $Ga_{Si}^{\{010\}}$ or $Al_{Si}^{\{010\}}$ will not have the transition from anomalous to normal since the p-factors increase with plane concentrations. Although there are temporary increases of $Ga_{Si}^{\{111\}}$ with $Ti_{Si}^{\{010\}}$ or $Sc_{Si}^{\{010\}}$ and $Sc_{Si}^{\{111\}}$ with $Ti_{Si}^{\{010\}}$ at a concentration of 6.25%, overall, the p-factors of $Al_{Si}^{\{111\}}$ with $Ti_{Si}^{\{010\}}$ or $Sc_{Si}^{\{010\}}$, $Ga_{Si}^{\{111\}}$ with $Ti_{Si}^{\{010\}}$ or $Sc_{Si}^{\{010\}}$, $Ti_{Si}^{\{111\}}$ with $Sc_{Si}^{\{010\}}$ and $Sc_{Si}^{\{111\}}$ with $Ti_{Si}^{\{010\}}$ decrease with concentrations and decline low enough to be smaller than $\sqrt{3}$ at the concentration of 25%, which means the transition will occur. In other words, when substituting atoms in both planes, $Ti_{Si}^{\{010\}}$ and $Sc_{Si}^{\{010\}}$ will change the anomalous behavior of yield stress to normal at the concentration of 25% no matter what atom is substituted in {111} planes, except $Ti_{Si}^{\{111\}}$, which makes the p -factor of $Ti_{Si}^{\{111\}\&\{010\}}$ be larger than $\sqrt{3}$. (see Figure 6). In contrast, to make the normalized Ni_3Si (see Figure 6) revert to anomalous, it is effective to substitute Al and Ga in {010} planes.

The p-factors of Al_3Sc are plotted in Figure 10: (a) $Ti_{Sc}^{\{111\}}$ with $Y_{Sc}^{\{010\}}$(black dashed-dotted line with circles), $Zr_{Sc}^{\{010\}}$ (purple solid line with triangles) and $Li_{Al}^{\{010\}}$ (red solid line with squares); (b) $Y_{Sc}^{\{111\}}$ with $Ti_{Sc}^{\{010\}}$ (black dashed-dotted line with circles), $Zr_{Sc}^{\{010\}}$ (purple solid line with squares) and $Li_{Al}^{\{010\}}$ (red solid line with triangles); (c) $Li_{Al}^{\{111\}}$ with $Ti_{Sc}^{\{010\}}$ (black dashed-dotted line with circles), $Y_{Sc}^{\{010\}}$ (red solid line with triangles) and $Zr_{Sc}^{\{010\}}$ (purple solid line with squares); (d) $Zr_{Sc}^{\{111\}}$ with $Ti_{Sc}^{\{010\}}$ (black dashed-dotted line with circles), $Y_{Sc}^{\{010\}}$ (red solid line with triangles) and $Li_{Sc}^{\{010\}}$ (purple solid line with squares), respectively.

From Figure 10, it is easy to see that only $Y_{Sc}^{\{111\}}$ with $Ti_{Sc}^{\{010\}}$ and $Zr_{Sc}^{\{111\}}$ with $Ti_{Sc}^{\{010\}}$ will have the transition from normal to anomalous at a concentration of 25%. p-factors of $Ti_{Sc}^{\{111\}}$ with $Zr_{Sc}^{\{010\}}$, $Li_{Al}^{\{010\}}$ or $Y_{Sc}^{\{010\}}$, $Y_{Sc}^{\{111\}}$ with $Zr_{Sc}^{\{010\}}$ or $Li_{Al}^{\{010\}}$, $Li_{Al}^{\{111\}}$ with $Ti_{Sc}^{\{010\}}$, $Zr_{Sc}^{\{010\}}$ or $Y_{Sc}^{\{010\}}$ and $Zr_{Sc}^{\{111\}}$ with $Li_{Al}^{\{010\}}$ or $Y_{Sc}^{\{010\}}$ stay lower than $\sqrt{3}$, though some of them increase with concentrations. Among them, the p-factor of $Li_{Al}^{\{111\}}$ with $Ti_{Sc}^{\{010\}}$ is close to $\sqrt{3}$ at the concentration of 25%. However, it still failed to overcome the critical value. Comparing to Figure 7, only $Ti_{Sc}^{\{010\}}$ at the concentration of 25% with Zr, Y or no atoms substituted in {111} planes may have the opportunity to change the property of yield

stress from normal to anomalous. This shows that $Ti_{Sc}^{\{010\}}$ has a great influence and makes the APB energies in {010} planes small enough to obtain a larger p-factor than $\sqrt{3}$. The only way to maintain the normal behavior is substituting Li or Ti (see Figure 7) in {111} planes.

Comparing to different concentrations, although it has influences on the p- factors, there are no obvious changes of the property of YSA varying from 6.25–12.5%. Only when the concentration is 25%, substitutional atoms can obviously change the property of yield stress between normal and anomalous such as $Sc_{Ge}^{\{111\}}$ with $Fe_{Ni}^{\{010\}}$, $Ga_{Si}^{\{111\}}$ with $Sc_{Si}^{\{010\}}$ and $Y_{Sc}^{\{111\}}$ with $Ti_{Sc}^{\{010\}}$.

5. Conclusions

The pressure-dependent elastic constants and APB energies of $L1_2$ intermetallics (Ni_3Ge, Ni_3Si, Al_3Sc, Ni_3Al, Ni_3Ga and Al_3Ti) are calculated using first-principles methods. Based on the energy criterion p-factor considering anisotropy, the properties of YSA under different pressures are predicted. Pressure will not introduce transition between anomalous and normal yield stress behavior. All these intermetallics are anomalous, except Al_3Sc. In order to obtain the transition in these intermetallics, the alloying elements are only substituted in Ni_3Ge, Ni_3Si, Al_3Sc due to their p-factors being close to $\sqrt{3}$. When Sc, Al or Ga is substituted in {111} planes in Ni_3Ge and Ni_3Si with the concentration of 25%, the anomalous Ni_3Ge and Ni_3Si will become normal. Based on the obtained normal Ni_3Ge and Ni_3Si, substituting Al or Ga in {010} planes with the concentration of 25%, the normal Ni_3Ge and Ni_3Si will revert to anomalous. $Ti_{Si}^{\{111\}}$ may have the same effect as Al and Ga. However, normal Al_3Sc will become anomalous when the concentration of $Ti_{Sc}^{\{010\}}$ is 25%. When Al in {111} planes is substituted by Li, the obtained anomalous Al_3Sc will become normal. Therefore, transition between normal and anomalous yield stress behavior can be introduced by alloying atoms in $L1_2$ intermetallics. Furthermore, when the plane concentration is lower than 6.25%, the transition will not occur. Until the concentration is larger or equal to 12.5%, the property may have the opportunity to be changed such as $Sc_{Ge}^{\{111\}}$, $Al_{Si}^{\{111\}}$ and $Ga_{Si}^{\{111\}}$. When the concentration is 25%, substitutional atoms will have much greater influences on the APB energies to change the property of yield stress between normal and anomalous more obviously, such as $Sc_{Si}^{\{111\}}$, $Ti_{Sc}^{\{010\}}$, $Ga_{Si}^{\{111\}}$ with $Sc_{Si}^{\{010\}}$ and $Y_{Sc}^{\{111\}}$ with $Ti_{Sc}^{\{010\}}$.

Author Contributions: Xiaozhi Wu and Jianwei Wang conceived and designed the ideas; Xiaojun Gao and Xiaozhi Wu performed the calculations; Rui Wang and Zhihong Jia analyzed the data; Jianwei Wang and Xiaojun Gao wrote the paper.

Conflicts of Interest: The authors declare no conflict of interest.

References

1. Westbrook, J.H. Defect structure and temperature dependence of hardness of an intermetallic compound. *Trans. TMS-AIME* **1957**, *209*, 898.
2. Flinn, P. Theory of deformation and superlattices. *Trans. TMS-AIME* **1960**, *218*, 145–154.
3. Davies, R.G.; Stoloff, N.S. Yield stress of aged Ni-Al alloys. *Trans. TMS-AIME* **1965**, *233*, 714.
4. Copley, S.M.; Kear, B.H. Working-hardening in off-stoichiometric. *Trans. TMS-AIME* **1967**, *239*, 977.
5. He, L.Z.; Zheng, Q.; Sun, X.F.; Hou, G.C.; Guan, H.R.; Hu, Z.Q. Low ductility at intermediate temperature of NiCbase superalloy M963. *Mater. Sci. Eng. A* **2004**, *380*, 340–348.
6. Sheng, L.Y.; Fang, Y.; Guo, J.T.; Xi, T.F. Anomalous yield and intermediate temperature brittleness behaviors of directionally solidified nickel-based superalloy. *Trans. Nonferrous Met. Soc.* **2014**, *24*, 673–681.
7. Chu, Z.K.; Yu, J.J.; Sun, X.F.; Guan, H.R.; Hu, Z.Q. Tensile property and deformation behavior of a directionally solidified Ni-base superalloy. *Mater. Sci. Eng. A* **2010**, *527*, 3010–3014.
8. Pope, D.P. *Physical Metallurgy*, 4th ed.; Elsevier Press: Amsterdam, The Netherlands, 1996; Volume 3, p. 2075.
9. Vitek, V.; Pope, D.P.; Bassani, J.L. *Disloactions in Solids*; Elsevier Press: Amsterdam, The Netherlands, 1996; Volume 10, p. 135.

10. Veyssière, P.; Saada, G.; Duesbery, M.S. *Disloactions in Solids*; Elsevier Press: Amsterdam, The Netherlands, 1996; Volume 10, p. 253.
11. Veyssière, P. Yield stress anomalies in ordered alloys: A review of microstructural findings and related hypotheses. *Mater. Sci. Eng. A* **2001**, *309*, 44–48.
12. Caillard, D.; Molénat, G.; Paidar, V. On the role of incomplete Kear-Wilsdorf locks in the yield stress anomaly of Ni_3Al. *Mater. Sci. Eng. A* **1997**, *234*, 695–698.
13. Bonneville, J.; Coupeau, C. Quantitative atomic force microscopy analysis of slip traces in Ni_3Al yield stress anomaly. *Mater. Sci. Eng. A* **2008**, *483*, 87–90.
14. Michel, J.; Coupeau, C.; Nahas, Y.; Drouet, M.; Beonneville, J. What can be learnt on the yield stress anomaly of Ni_3Al using AFM observations. *Intermetallics* **2014**, *50*, 86–93.
15. Caillard, D.; Couret, A. *Disloactions in Solids*; Elsevier Press: Amsterdam, The Netherlands, 1996; Volume 10, p. 69.
16. Rao, S.I.; Dimiduk, D.M.; Parthasarathy, T.A.; Unchic, M.D.; Woodward, C. Atomistic simulations of intersection cross-slip nucleation in $L1_2$ Ni_3Al. *Scr. Mater.* **2012**, *66*, 410–413.
17. Paidar, V.; Pope, D.P.; Vitek, V. A theory of the anomalous yield behavior in $L1_2$ ordered alloys. *Acta Metall.* **1984**, *32*, 435–448.
18. Umakoshi, Y.; Pope, D.P.; Vitek, V. The asymmetry of the flow stress in Ni_3(Al,Ta) single crystals. *Acta Metall.* **1984**, *32*, 449–456.
19. Kear, B.H.; Wilsdolf, H.G. Dislocation configurations in plastically deformed polycrystalline Cu_3Au alloys. *Trans. Metall. Soc. AIME* **1962**, *224*, 382.
20. Gorbatov, O.I.; Lomaev, I.L.; Gornostyrev, Y.N. Effect of composition on antiphase boundary energy in Ni_3Al based alloys: Ab initio calculations. *Phys. Rev. B* **2016**, *93*, 224106.
21. Sun, R.; Van de Walle, A. Automating impurity-enhanced antiphase boundary energy calculations from ab initio Monte Carlo. *CALPHAD* **2016**, *53*, 20–24.
22. Koizumi, Y.; Mizuno, M.; Sugihara, A. Effects of substitutional impurity Au and Si atoms on antiphase boundary energies in Ti_3Al: A first principles study. *Philos. Mag.* **2010**, *90*, 3919–3934.
23. Vamsi, K.V.; Karthikeyan, S. MATEC Web of Conferences. **2014**, *14*, 11005.
24. Shoeck, G.; Kohlhammer, S.; Fähnle, M. Planar dissociations and recombination energy of [110] superdislocations in Ni_3Al: Generalized Peierls model in combination with ab initioelectron theory. *Philos. Mag. Lett.* **1999**, *79*, 849–857.
25. Yoo, M.H. On the theory of anomalous yield behavior of Ni_3Al-effect of elastic anisotropy. *Scr. Metall.* **1986**, *20*, 915.
26. Paxton, A.T.; Sun,Y.Q. The role of planar fault energy in the yield anomaly in $L1_2$ intermetallics. *Philos. Mag. A* **1998**, *78*, 85–104.
27. Kumar, K.; Sankarasubramanian, R.; Waghmare, U.V. The effect of $\gamma - \gamma'$ interface on the tensile and shear strengths of nickel-based superalloys: A first-principles study. *Comput. Mater. Sci.* **2015**, *97*, 26–31.
28. Manga, V.R.; Shang, S.L.; Wang, W.Y.; Wang, Y.; Liang, J.; Crespi, V.H.; Liu, Z.K. Anomalous phonon stiffening associated with the (111) antiphase boundary in $L1_2$ Ni_3Al Original research article. *Acta Mater.* **2015**, *82*, 287–294.
29. Demura, M.; Golberg, D.; Hirano, T. An athermal deformation model of the yield stress anomaly in Ni_3Al. *Intermetallics* **2007**, *15*, 1322–1331.
30. Abzaev, Y.A.; Starenchenko, V.A.; Solo'eva, Y.V.; Kozlov, E.V. Effect of orientation on the peak temperature of the yield-stress anomaly in single crystals of the Ni_3Ge alloy. *Phys. Met. Metall.* **2006**, *101*, 591–595.
31. Suzuki, T.; Oya, Y.; Wee, D.M. Transition from positive to negative temperature dependence of the strength in Ni_3Ge-Fe_3Ge solid solution. *Acta Metall.* **1980**, *28*, 301–310.
32. Pak, H.R.; Saubri, T.; Nenno, S. Temperature and Orientation Dependence of the Yield Stress in Ni_3Ge Single Crystals. *Trans. Jpn. Inst. Met.* **1977**, *18*, 617–626.

33. Thornton, P.H.; Davies, R.G. The temperature dependence of the flow stress of gamma prime phases having the Ll_2 structure. *Metall. Trans.* **1970**, *1*, 549–550.
34. Dyck, S.V.; Delaey, L.; Froyen, L.; Buekenhout, L. Microstructural evolution and its influence on the mechanical properties of a nickel silicide based intermetallic alloy. *Intermetallics* **1997**, *5*, 137–145.
35. Takasugi, T.; Yoshida, M. Strength anomaly and dislocation structure at 4.2 k in ni_3(si, ti) single crystals. *Philos. Mag. A* **1992**, *65*, 613–624.
36. Lunt, M.J.; Sun, Y.Q. Creep and the anomalous yield stress of Ni_3Ga. *Mater. Sci. Eng. A* **1997**, *239*, 445–449.
37. Takeuchi, S.; Kuramoto, E. Anomalous Temperature Dependence of the Yield Stress in Ni_3Ga. *J. Phys. Soc. Jpn.* **1971**, *31*, 1282.
38. Takeuchi, S.; Kuramoto, E. Temperature and orientation dependence of the yield stress in Niin3Ga single crystals. *Acta Metall.* **1973**, *21*, 415–425.
39. Wu, Z.L.; Pope, D.P.; Vitek, V. Deformation and fracture of $L1_2$ $(Al,Fe)_3Ti$. *Scr. Metall.* **1990**, *24*, 2187.
40. Geng, P.J.; Li, W.G.; Zhang, X.H.; Deng, Y.; Kou, H.B.; Ma, J.Z.; Shao, J.X.; Chen, L.M.; Wu, X.Z. A theoretical model for yield strength anomaly of Ni-base superalloys at elevated temperature. *J. Alloy. Compd.* **2017**, *706*, 340–343.
41. Liu, J.B.; Johnson, D.D.; Smirnov, A.V. Predicting yield-stress anomalies in $L1_2$ alloys: Ni_3Ge-Fe_3Ge pseudo-binaries. *Acta Mater.* **2005**, *53*, 3601–3612.
42. Hagihara, K.; Tanaka, T.; Nakano, T.;Veyssière, P.; Umakoshi, Y. Effects of the anisotropy of the anti-phase boundary energy on the yield-stress anomaly in Ni_3X compounds with close-packed crystal structures. *Philos. Mag. Lett.* **2007**, *87*, 705–712.
43. Hagihara, K.; Tanaka, T.; Izumo, H.; Umakoshi, Y.; Nakano, T. Non-basal slip in Ni_3(Ti, Nb) and Ni_3(Ti, Al) single crystals with various long-period stacking ordered structures. *Acta Mater.* **2013**, *61*, 4365.
44. Nishino, Y.; Tanahashi, T. Effect of molybdenum substitution on the yield stress anomaly in Fe_3Al-based alloys. *Mater. Sci. Eng. A* **2004**, *387*, 973–976.
45. George, E.P.; Baker, I. Thermal vacancies and the yield anomaly of FeAl. *Intermetallics* **1998**, *6*, 759–763.
46. Mitchell, T.E.; Baskes, M.I.; Hoagland, R.G.; Misra, A. Dislocation core structures and yield stress anomalies in molybdenum disilicide. *Intermetallics* **2001**, *9*, 849–856.
47. Nakano, T.; Hagihara, K. Yield stress anomaly controlled by the phase stability in $NbSi_2$ single crystals. *Scr. Mater.* **2013**, *68*, 313–316.
48. Liu, L.L.; Wu, X.Z.; Wang, R.; Li, W.G.; Liu, Q. Stacking fault energy, yield stress anomaly, and twinnability of Ni_3Al: A first principle study. *Chin. Phys. B* **2015**, *24*, 077102.
49. Lü, B.L.; Chen, G.Q.; Qu, S.; Su, H.; Zhou, W.L. First-principle calculation of yield stress anomaly of Ni_3Al-based alloys. *Mater. Sci. Eng. A* **2013**, *565*, 317–320.
50. Golovin, I.S.; Jäger, S.; Mennerich, C.; Siemers, C.; Neuhäuser, H. Structure and anelasticity of Fe_3Ge alloy. *Intermetallics* **2007**, *15*, 1548–1557.
51. Balk, T.J.; Kumar, M.; Hemker, J. Influence of Fe substitutions on the deformation behavior and fault energies of Ni_3Ge-Fe_3Ge $L1_2$ intermetallic alloys. *Acta Mater.* **2001**, *49*, 1725–1736.
52. Hu, W.C.; Liu, Y.; Li, D.J.; Zeng, X.Q.; Xu, C.S. Mechanical and thermodynamic properties of Al_3Sc and Al_3Li precipitates in Al-Li-Sc alloys from first-principles calculations. *Phys. B* **2013**, *427*, 85–90.
53. Saal, J.E.; Wolverton, C. Energetics of antiphase boundaries in γ' Co_3(Al,W)-based superalloys. *Acta Mater.* **2016**, *103*, 57–62.
54. Wu, X.Z.; Wang, R.; Wang, S.F.; Wei, Q.Y. Ab initio calculations of generalized-stacking-fault energy surfaces and surface energies for FCC metals. *Appl. Surf. Sci.* **2010**, *256*, 6345–6349.
55. Frankel, J.; Vassiliou, J.; Jamieson, J.C.; Dandekar, D.P.; Scholz, W. The elastic constants of Ni_3Al to 1.4 GPa. *Physica B+C* **1986**, *139*, 198–201.
56. Duan, Y.H.; Sun, Y.; Peng, M.J.; Zhou, S.G. Ab-initio investigations on elastic properties in $L1_2$ structure Al3Sc and Al_3Y under high pressure. *J. Alloy. Compd.* **2014**, *585*, 587–593.
57. Boucetta, S.; Zegrar, F. First-Principles Study of the Structural, Elastic, and Mechanical Properties of Ni_3Ga Compound under Pressure. *Acta Phys. Pol. A* **2014**, *125*, 54.
58. Pearson, W.B. *A Handbook of Lattice Spacings and Structures of Metals and Alloys*; Pergamon Press: Pergamon, Turkey; New York, NY, USA, 1958.
59. Li, J.; Zhang, M.; Luo, X. Theoretical investigations on phase stability, elastic constants and electronic structures of $D0_{22}$- and $L1_2$-Al_3Ti under high pressure. *J. Alloy. Compd.* **2013**, *556*, 214–220.

60. Tian, T.; Wang, X.F.; Li, W. Ab initio calculations on elastic properties in $L1_2$ structure Al_3X and X_3Al-type (X = transition or main group metal) intermetallic compounds. *Solid State Commun.* **2013**, *156*, 69–75.
61. Fu, C.L.; Ye, Y.Y.; Yoo, M.H. Theoretical investigation of the elastic constants and shear fault energies of Ni_3Si. *Philos. Mag. Lett.* **1993**, *67*, 179–185.